




# Effect of zirconium on precursor chemistry, phase stability, and oxidation of polyvinylsilazane-derived SiCN ceramics

Rahul Anand<sup>1</sup>, Bibhuti B. Nayak<sup>1</sup>, and Shantanu K. Behera<sup>1,\*</sup> 

<sup>1</sup>Laboratory for New Ceramics, Department of Ceramic Engineering, National Institute of Technology Rourkela, Rourkela, Odisha 769008, India

**Received:** 10 April 2021

**Accepted:** 9 November 2021

**Published online:**

3 January 2022

© The Author(s), under exclusive licence to Springer Science+Business Media, LLC, part of Springer Nature 2021

## ABSTRACT

The present work focuses on the structural changes of polyvinylsilazane precursor upon modification by a molecular precursor of zirconium and processing of high temperature stable nanostructured SiCN and SiZrCNO ceramics. The bonding characteristics of the polymerized as well as pyrolyzed samples of pure and Zr-modified polyvinylsilazane precursor and their polymer to ceramic conversion processes have been analyzed. Zr doping shifts the ceramization process to an earlier temperature as compared to the undoped preceramic polymer. The structural evolution of metastable SiCN and SiZrCNO systems was studied by using X-ray diffraction, high-resolution transmission electron microscopy, and diffraction intensity profiles. The pure SiCN system remained as a single-phase amorphous ceramic up to 1400 °C. While the Zr-doped SiCN ceramics also appeared as monophasic amorphous ceramic at 1000 °C, nanocrystals of t-ZrO<sub>2</sub> were found to precipitate throughout the ceramic microstructure with exceptional homogeneity for samples pyrolyzed at higher temperatures. The high temperature stability of t-ZrO<sub>2</sub> in the amorphous SiCN matrix has also been demonstrated. Constant rate heating oxidation studies indicated remarkable improvement in mass retention of the Zr-doped SiCN system as compared to the undoped ceramic for temperatures as high as 1500 °C. The retention of tetragonal phase of ZrO<sub>2</sub> in the ceramic matrix, even after pyrolysis at 1400 °C and improved oxidation resistance provide significant advantages for achieving tough and thermally stable SiCN-ZrO<sub>2</sub> ceramic nanocomposites for bond coat applications.

Handling Editor: N. Ravishankar.

Address correspondence to E-mail: Behera@alum.lehigh.edu

<https://doi.org/10.1007/s10853-021-06780-7>

## Introduction

Requirement of highly fuel efficient and environmentally benign gas turbine engines has warranted exploration of high temperature resistant materials systems [1, 2]. To mitigate the demands of high inlet gas temperatures ceramic matrix composites (CMC) of SiC, SiC fiber reinforced ceramic composites (SiC–SiC),  $\text{Si}_3\text{N}_4$  monoliths, etc., are being considered [2–4]. However, SiC-based materials are unstable in high temperature gas environment containing moisture and lead to severe materials recession [5, 6]. Therefore, it is necessary to protect the carbide-based CMC with an environmental barrier coating (EBC) [1]. Development of materials systems for EBC has enormous challenges with a series of prerequisites for its qualification, and over the years, many ceramics have been explored [7].  $\text{ZrO}_2$ - and  $\text{HfO}_2$ -based systems have evolved as preferred choices due primarily to their water vapor induced recession being extremely minimal in high temperature environments [6, 8]. Nevertheless, the relatively large coefficient of thermal expansion (CTE) of  $\text{ZrO}_2$  and  $\text{HfO}_2$  as compared to that of SiC-based CMC is a concern. Large differences in CTE build thermal stresses during cyclic operations across a large temperature range causing spalling and damage of the components. Such problems of the difference in CTE and a perfect bonding between an oxide coating and a non-oxide ceramic substrate system can be mitigated with the development of an intermediate layer that has character of both the substrate and the coating. Since the intermediate coating layer is of a few microns, the constituent material phases must be distributed at an extremely fine nanostructured level. This work is presented on the development of such a nonoxide-oxide nanocomposite system derived from preceramic polymers.

Precursor-derived ceramics (PDC), prepared by inert pyrolysis of Si-containing polymers, are novel, yet complex, nanostructured ceramics that possess excellent thermo-mechanical properties, such as resistance to creep, oxidation, and corrosion [9–14]. The exceptional properties, along with the ability of being shaped by various fabrication techniques, have enabled its application in numerous sectors, including environmental systems, biomedical components, anode material in lithium batteries, aerospace, and defense [15]. The preceramic monomer governs the

composition, phase, and microstructure of the final ceramic, and thus its properties as well. Polymer-derived silicon carbonitride (SiCN) ceramics have great tolerance to oxygen without any deterioration in their thermal stability and creep [14]. Low to moderate temperature thermolysis of preceramic polymer makes its constituent atoms arrange in a single-phase amorphous structure [16]. Annealing of the SiCN ceramic beyond 1440 °C leads to the formation of  $\text{Si}_3\text{N}_4$  and turbostratic carbon in the nanostructure [17, 18]. Also, in the metastable SiCN system, the excess carbon reacts with  $\text{Si}_3\text{N}_4$  to form SiC and  $\text{N}_2$  at temperatures above 1450 °C [19, 20]. The excess residual carbon present in SiCN system hinders or slows down the crystallization by blocking diffusion [21]. Similarly, amorphous to crystalline transformation has been observed in many preceramic polymer-derived systems, such as SiC, SiCN, SiCO, SiCNO, and SiBCN [22–24]. Interestingly, changes in the properties have been observed in ceramic systems by incorporating the preceramic polymers with molecular sources of reactive elements [25–27]. In Ti-doped SiOC system, Ti accelerates SiC formation in the SiOC matrix and precipitates as TiC, thus improving oxidation resistance [25]. Incorporation of  $\text{ZrO}_2$  into polymer-derived SiOC ceramics also has been found to improve its crystallization and decomposition temperature exceeding 1300 °C [27]. Linck et al. investigated hydrothermal corrosion of SiZrOC and SiHfOC ceramics at moderate temperature and observed improved resistance as compared to SiC, SiOC and  $\text{Si}_3\text{N}_4$  [28]. Lately, doping rare earth cations, such as Zr and Hf, in the SiCN matrix, SiZrCNO and SiHfSCNO hybrid systems with improved thermostructural properties have also been fabricated [29–33]. However, a distributed oxide phase in a nonoxide ceramic matrix with improved uniformity and homogeneity is the cornerstone of such high temperature resistant materials systems for an intermediate coating.

In this work, molecular precursor-derived  $\text{ZrO}_2$  phase is co-developed with a precursor polymer-derived silicon carbonitride (SiCN) ceramic, thus forming a nanostructured SiCN- $\text{ZrO}_2$  composite. The main concern of  $\text{ZrO}_2$  is its transformation to different polymorphs [34]. Tetragonal zirconia converts to monoclinic phase above 1170 °C causing considerable volume change ( $\sim 4$  vol% increase) and shear strain (14–15%), which can lead to structural deformation. On the contrary, if the tetragonal form of

ZrO<sub>2</sub> can be stabilized, the materials microstructure can make use of transformation toughening mechanism for enhanced fracture toughness [35]. Therefore, the objective of the current work is to explore the precursor architecture of a polyvinylsilazane modified through Zr, high temperature evolution of phase and microstructure, and their stability. Understanding the molecular modifications of the preceramic polymer leading to the microstructure evolution process of such multicomponent pseudo-amorphous systems can be quite challenging, which has been carried out in this work with analytical characterization tools, including X-ray diffraction (XRD), transmission electron microscopy (TEM) and high-resolution TEM (HRTEM). Further, thermal stability of the nanocomposites in oxidizing atmosphere has also been investigated using constant heating rate thermogravimetry (TGA) and Raman spectroscopy.

## Experimental

A commercially available polyvinylsilazane (PVS, Durazane®1800, Merck Chemicals, Germany) was blended with 1 wt% of crosslinking agent (dicumyl peroxide, DCP, Sigma-Aldrich®) and thermally crosslinked in flowing nitrogen atmosphere at 300 °C for 2 h with a heating rate 2 °C min<sup>-1</sup> from room to peak temperature, followed by natural cooling. The obtained glassy material was crushed to powders with the help of a high energy mill (Spex 8000 M, Spex SamplePrep, Metuchen, NJ, USA). The cross-linked powder was pyrolyzed in an alumina tube furnace at various temperatures ranging from 1000 to 1400 °C for different times ranging from 2 to 6 h in flowing nitrogen atmosphere. These ceramics obtained after the inter pyrolysis of PVS precursors are referred to as SiCN ceramics. Likewise, the Zr-doped PVS (Zr-PVS) precursors upon pyrolysis are referred to as SiZrCNO ceramics. For the synthesis of SiZrCNO, 20 wt% zirconium (IV) n-propoxide (Sigma-Aldrich®) solution was added along with polyvinylsilazane and DCP. The blended solution was crosslinked and pyrolyzed in the same condition as mentioned for the synthesis of SiCN. The pyrolytic conversion of the preceramic polymer was investigated using several analytical techniques. The mass changes with temperature of the crosslinked precursors were determined by thermogravimetric analysis (Netzsch, Germany, STA/TG-DSC) under inert

atmosphere for yield estimation. Furthermore, differential scanning calorimetry (DSC) was performed to investigate the thermal aspects of the polymer to ceramic conversion, phase separation and crystallization phenomena in various compositions. Fourier transform infrared spectroscopy (FTIR, Spectrum II, Perkin Elmer) was employed to study the structural modification in the polymer upon addition of the dopant at different stages of heat treatment by analyzing the characteristic bond vibrations. For analysis, the powder samples were mixed with KBr (Sigma-Aldrich®) in 1:10 ratio and pressed to pellets using a hydraulic press. X-ray diffraction (Ultima IV, Rigaku, Japan) analysis of the pyrolyzed specimens was performed using Cu K $\alpha$  radiation ( $\lambda = 0.154$  nm). To understand the evolution of nanostructure of SiCN and SiZrCNO ceramic matrix, bright-field and high-resolution imaging was performed using TEM (Technai G<sup>2</sup>, FEI, Eindhoven, NL) at an accelerating voltage of 300 kV. The powdered samples were dispersed in isopropanol, ultrasonicated, and drop-cast on a carbon coated copper grid (300 mesh, Ted Pella, USA). For analysis of the high-resolution TEM micrographs (HRTEM), Gatan Digital Micrograph® software was used. The lattice fringes were calculated applying the fast Fourier-transform (FFT) algorithm on selected areas over the micrograph of the lattice fringes in the crystallite. After computation, the fringe width was measured from the inverse FFT image derived from the micrograph. Further, oxidation of the undoped and Zr-doped SiCN powders was studied up to 1500 °C using thermogravimetric analysis (TGA) in flowing oxygen atmosphere with a constant heating rate of 5 °C min<sup>-1</sup>. The oxygen flow rate was maintained uniform with 80 ml s<sup>-1</sup> throughout the oxidation process. Furthermore, the 1400 °C pyrolyzed pure SiCN and Zr-doped SiCN ceramics were oxidized in an open hearth furnace at 1400 °C for 2 h. Raman spectroscopy of the pyrolyzed and oxidized samples was done to understand the effect of Zr on the existence and role of carbon in SiCN during oxidation. Raman spectroscopy (XMB3000, WITec GmbH, Germany) was performed on powdered samples using a monochromatic argon laser beam of 532 nm wavelength and power ranged 0.001 mW–0.002 mW for 60 s in 1000 to 3300 cm<sup>-1</sup> spectral range.

## Results and discussion

The thermal behavior of the crosslinked undoped and Zr-modified PVS precursors, investigated between room temperature and 1400 °C, is shown in Fig. 1. The undoped PVS precursor shows single step mass loss in between 400 and 800 °C (c.f. Figure 1a). The mass loss is mainly due to the loss of hydrogen and  $C_nH_m$  hydrocarbons caused by decomposition of polymeric chain of the crosslinked precursor [36]. The yield was estimated to be 82.80% for pure PVS precursor. The TGA curve shows two weight loss steps for the Zr-PVS precursor indicating reduced ceramic yield as compared to the unmodified PVS precursor (c.f. Figure 1a). For the Zr modified sample, the first mass loss step (with a loss of 17.20%) can be considered in between 300 to 700 °C, which corresponds to the loss of hydrogen and various hydrocarbons ( $C_nH_m$ ). A minor mass loss of 3.50% occurs during second step in temperature between 1200 and 1400 °C. This loss is mainly related to the loss of excess stoichiometric oxygen (with respect to  $ZrO_2$ ) present in Zr-propoxide. The Zr modification to the PVS accelerates its conversion rate to form a ceramic. The conversion process of pure PVS and Zr-PVS precursors to ceramics in a nitrogen atmosphere was completed at 800 °C and 700 °C, respectively. The early ceramization of Zr-PVS precursor can be attributed to the high reactivity of Zr atoms towards the Si–N and Si–C bonds, which eventually leads to the cleavage of these bonds at lower temperature.

Similar results have been reported by Dirè et.al. in a Ti modified polydimethylsiloxane system [36, 37]. The overall ceramic yields of the pure PVS and Zr-PVS precursors crosslinked sample were found to be ~ 82.8 wt% and 79.3 wt%, respectively.

Figure 1b shows the DSC curves of undoped PVS and Zr-PVS precursors. A sharp rise of the curve could be observed at 780 °C for the undoped PVS system that is attributed to the transformation of the sample from polymeric to glassy state. In the DSC curve of Zr-PVS precursor, the small peak at 350 °C and a sharp exothermic peak at 590 °C may be due to the polymerization reactions of  $(H_7C_3-O)_4-Zr$  molecule to -Si–H sites and polymer to ceramic transformation. The DSC curve of PVS shows an exothermic peak at around 1180 °C, which can be attributed to the local crystallization of carbon nanodomains in the SiCN matrix. The same exothermic peak could be observed more prominently in the DSC curve of Zr-PVS sample. The relatively sharper exothermic peak may be attributed to the nucleation of  $ZrO_2$  crystals in the SiCN matrix. The small peak above 1370 °C in the PVS system may be due to the initiation of phase separation and local crystallization of the amorphous SiCN ceramics.

The FTIR spectra of undoped PVS and Zr-PVS heat treated at different processing temperatures are shown in Fig. 2. Here, the vinyl stretching bands disappeared for samples crosslinked at 300 °C implying early start of crosslinking due to vinyl group polymerization (Fig. 2a and b). The band at

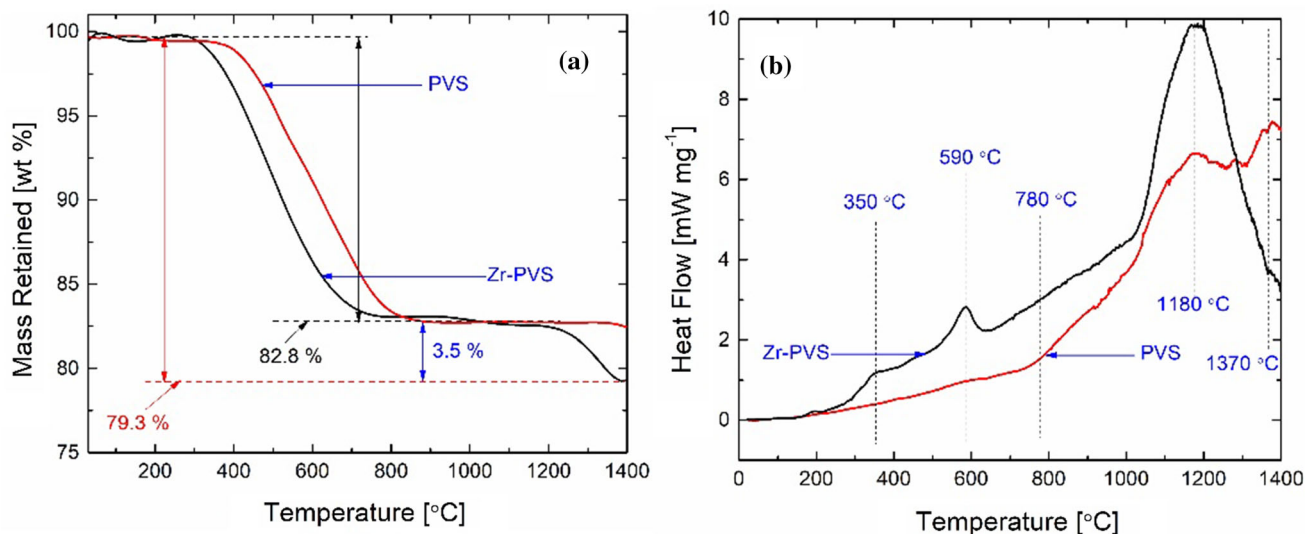


**Figure 1** Thermal behavior of the crosslinked PVS and Zr-doped PVS precursors; **a** Thermogravimetric analysis, and **b** Differential scanning calorimetry.



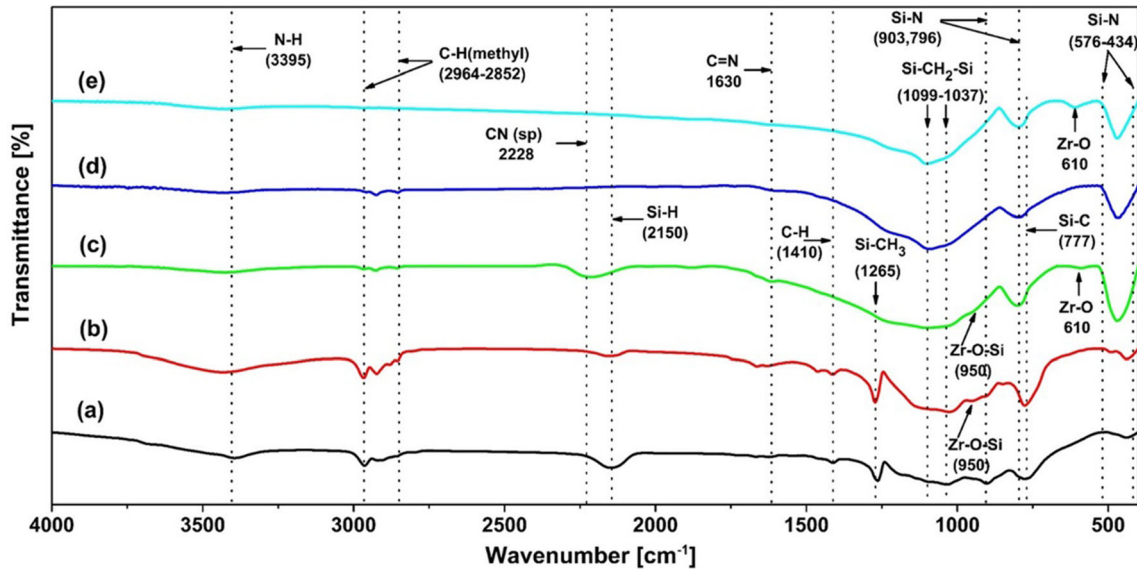


**Figure 2** FTIR analysis of samples pyrolyzed at different temperatures; **a** Undoped PVS crosslinked at 300 °C, **b** Zr-PVS crosslinked at 300 °C, **c** Zr-PVS pyrolyzed at 1000 °C, **d** PVS pyrolyzed at 1300 °C (i.e. SiCN), and **e** Zr-PVS pyrolyzed at 1300 °C (i.e. SiZrCNO).

$3395\text{ cm}^{-1}$  corresponds to the stretching mode of  $\text{-NH-}$  in  $\text{Si-NH-Si}$ , which reduced significantly above  $300\text{ °C}$  indicating the important crosslinking reactions of cyclic  $\text{Si-N-Si}$  bond formation [38, 39]. The absorption peaks ranging from  $2964$  to  $2852\text{ cm}^{-1}$  are due to the stretching of  $\text{C-H}$  bond ( $\text{-CH}_3$  unit) [32]. The absorption in the range of  $1099\text{--}1037\text{ cm}^{-1}$  corresponds to the stretching mode of  $\text{Si-O}$  band and wagging mode of  $\text{-CH}_2\text{-}$  band in present  $\text{-Si-CH}_2\text{-}$  /  $\text{-Si-CH(R)-Si-}$ . The absorption bands at  $2150\text{ cm}^{-1}$ ,  $1410\text{ cm}^{-1}$ , and  $1265\text{ cm}^{-1}$  are attributed to the stretching mode of  $\text{-Si-H}$ ,  $\text{-C-H}$ , and  $\text{-Si-CH}_3$  bands, respectively. Intensity of these absorption bands decreases with rise in the pyrolysis temperature and disappears for samples pyrolyzed above  $1000\text{ °C}$  indicating polymer to ceramic conversion. It is remarkable that hydrogen remains in the ceramic matrix attached with carbon and silicon molecules even at  $1000\text{ °C}$  (Fig. 2c). The additional absorption band at  $950\text{ cm}^{-1}$  may be ascribed to  $\text{Zr-O-Si}$ , as has been reported in the literature for absorption peaks in similar ranges [26, 32, 40, 41]. It has also been observed that the  $\text{Zr-O-Si}$  bonds remain intact even for the  $\text{SiZrCNO}$  ceramic pyrolyzed at  $1000\text{ °C}$  (Fig. 2c). The absorption peak at  $1630\text{ cm}^{-1}$  resembles  $\text{C}=\text{N}$  stretching vibration (sample pyrolyzed at  $1000\text{ °C}$ ) and can presumably be a nitrogen containing graphene-like structure [42, 43]. The peak intensity of  $\text{C}=\text{N}$  bond starts weakening at higher

temperature indicating decrease in graphite content [44]. Similarly, the weak absorption band corresponding to  $2228\text{ cm}^{-1}$  is ascribed to the existence of  $\text{C}\equiv\text{N}$  (sp hybridization) stretching vibration, which is found for the  $1000\text{ °C}$  pyrolyzed ceramic (Fig. 2c) and eliminated at higher temperature [45, 46]. The peak at  $777\text{ cm}^{-1}$  corresponds to asymmetric stretching vibration mode of  $\text{-Si-C-}$  bond [44, 47].

The peak corresponding to  $610\text{ cm}^{-1}$  shows the presence of the  $\text{Zr-O}$  bond since the band intensity for this peak rises with temperature for Zr-doped pyrolyzed samples (Fig. 2c and e). The absorption at  $610\text{ cm}^{-1}$  is conspicuous by its absence for the pyrolyzed pure SiCN sample (Fig. 2d). The absorption peaks at  $796\text{ cm}^{-1}$  and  $903\text{ cm}^{-1}$  refer to asymmetric stretching of  $\text{-N-Si-N-}$  bond in  $\text{-Si-N}_4$  and  $\text{-N-Si}_3$  units, respectively [48–50]. The peaks between  $434\text{--}567\text{ cm}^{-1}$  (Fig. 2c) can be attributed to the stretching modes of the distorted  $\text{-Si-N-}$  bonds [44].

Based on the FTIR spectroscopic information, probable crosslinking reaction mechanisms for polymerization of pure PVS and Zr-PVS precursors are proposed in Fig. 3. The reaction initiates due to DCP which provides phenyl and methyl free radicals after thermal decomposition (Reaction (a), Fig. 3). The possible reaction paths for free radical polymerization are shown in reaction (b) and (c) (cf. Figure 3). These free radicals react with the vinyl containing monomer of vinylsilazane and generate a free radical

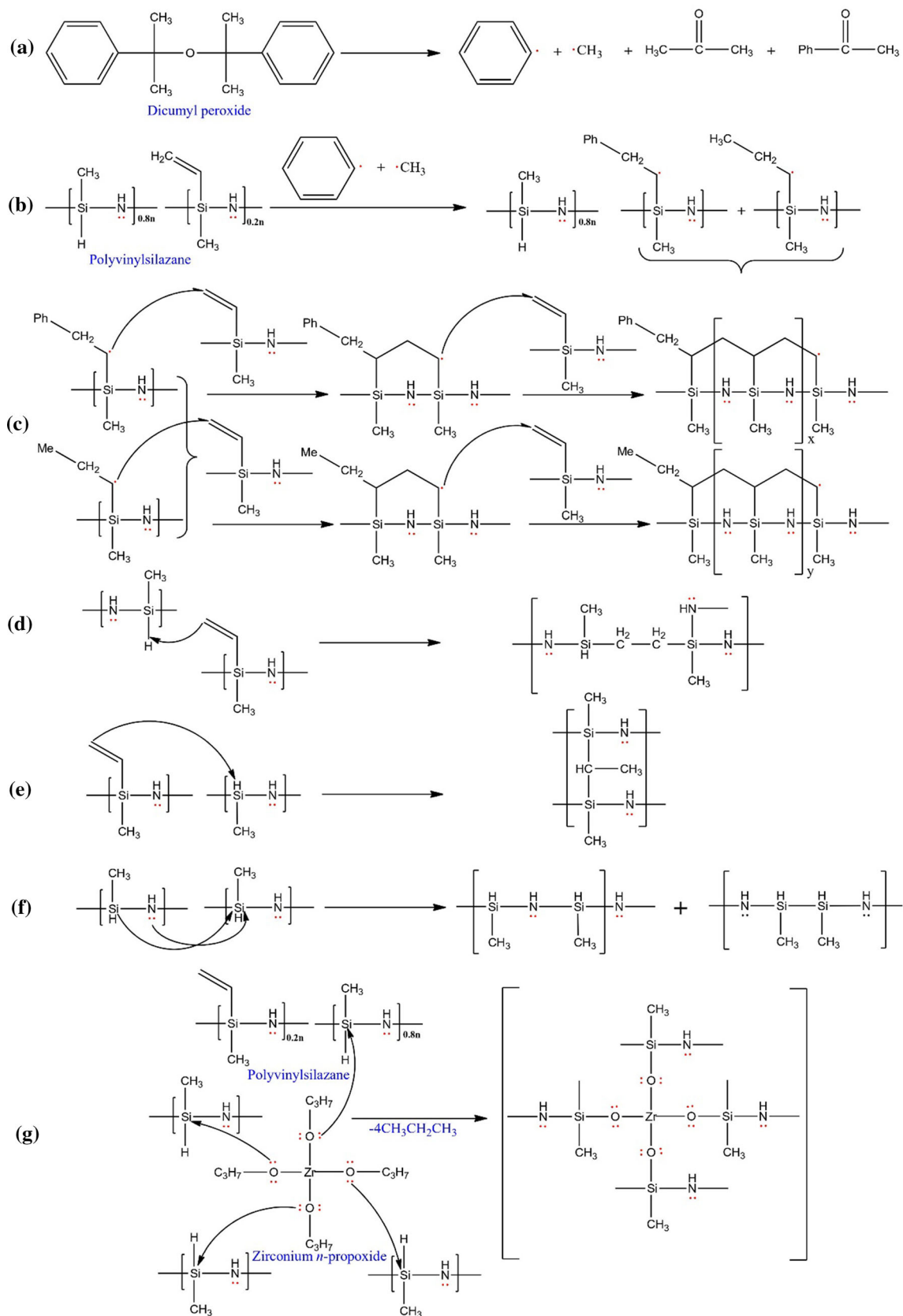


**Figure 3** Probable reaction mechanisms in pure PVS and Zr-PVS precursors during crosslinking.

on 2° carbon linked to silicon (Reaction (b), Fig. 3). The subsequent free radical containing groups react and combine to other intact vinyl monomer units starting a chain polymerization (Reaction (c), Fig. 3). The phenyl containing chains formed are major product as compared to methyl as the free radical on phenyl are more stable (due to resonance effect) than on methyl. Further, two different monomer units of PVS may combine by simple addition of vinyl group and  $-\text{Si}-\text{H}$  sites to form a linear polymeric chain containing  $-\text{Si}-\text{CH}_2-\text{CH}_2-$  and  $-\text{Si}-\text{CHCH}_3-\text{Si}-$  units, respectively (Reaction (d) and (e), Fig. 3). In addition, self-polymerization also occurs following reaction in undoped PVS system and forms  $-\text{Si}-\text{NH}-\text{Si}-$  and  $-\text{N}-\text{SiH}(\text{CH}_3)-\text{SiH}(\text{CH}_3)-\text{N}-$  linear/cyclic chains (Reaction (f), Fig. 3). These polymeric chains during pyrolysis form different units containing Si, C, and N leading to the formation of a nanostructured ternary  $\text{SiC}_x\text{N}_y$  hybrid ceramic.

The reaction pathway for the Zr-PVS is shown in reaction (g) following nucleophilic substitution reaction (Fig. 3). One molecule of Zr precursor may react with maximum 4 monomer units of PVS containing reactive  $-\text{Si}-\text{H}$  site. Moreover, consequential Zr containing monomer unit reacts to the vinyl group,  $-\text{Si}-\text{H}$  and  $-\text{N}-\text{H}$  sites of monomers via similar radical and different addition reaction paths as shown in reaction mechanism (b) to (e) of undoped PVS precursor. Here, the Zr and O will add to the basic forming units along with Si, C, and N leading to the formation of Si-Zr-O-C-N hybrid ceramic.

Phase evolution and crystallization behavior of the SiCN and SiZrCNO ceramics thus derived were studied by X-ray diffraction (Fig. 4). The SiCN ceramics were found to be primarily amorphous up to 1400 °C. However, faint peaks at  $2\theta \sim 25.5$  and  $44^\circ$  degrees, corresponding to the (002) and (110) planes of graphite (JCPDS #75–1621), respectively, indicate the presence of residual carbon in the SiCN ceramics pyrolyzed at 1400 °C. Extremely small peaks of nanocrystalline  $\alpha\text{-Si}_3\text{N}_4$  (JCPDS #09–0250) at Bragg angles 35.0, 43.3, 57.5, and 66.5 degrees corresponding to planes (210), (301), (222), and (004), respectively, can also be noticed in the same SiCN sample. The XRD patterns of the SiZrCNO samples annealed from 1000 to 1400 °C also exhibit largely amorphous nature. For the SiZrCNO samples, the separation of nanosized  $\text{ZrO}_2$  (JCPDS #79–1771) phase was detected for the 1200 °C pyrolyzed sample. The diffraction peaks at  $2\theta$  in the vicinity of  $30^\circ$ ,

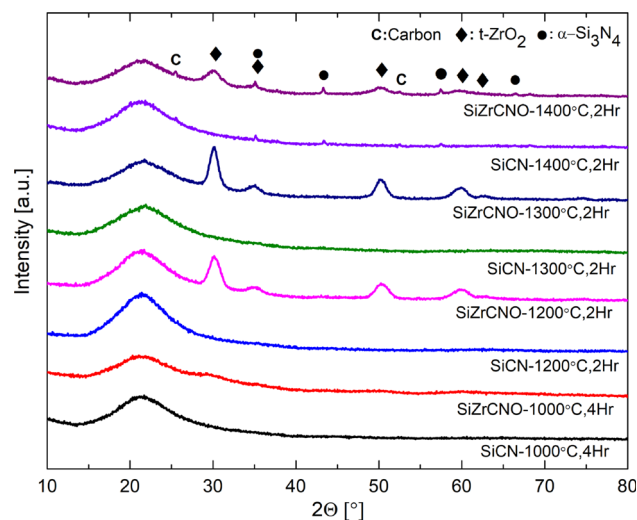


**Figure 4** X-ray diffraction patterns of SiCN and SiZrCNO ceramics prepared at temperature ranging from 1000 to 1400 °C.

$35^\circ$ ,  $50^\circ$  and  $60^\circ$  correspond to (101), (110), (112) and (211) planes, respectively, and confirm the presence of tetragonal phase of  $\text{ZrO}_2$ . For the SiZrCNO sample pyrolyzed at 1400 °C, faint peaks of residual graphitic carbon and nanocrystalline  $\alpha\text{-Si}_3\text{N}_4$  (JCPDS #09–0250) have also been observed. The crystallite size of  $t\text{-ZrO}_2$  calculated for the samples pyrolyzed at various temperatures by Scherrer's formula was found to be in the range of 4.6 to 7.8 nm.

Electron microscopic analysis of the prepared ceramic specimens was performed to understand their thermal stability and crystallization process. The SiCN samples pyrolyzed at 1000 °C for 4 h exhibited no appreciable contrast through transmission electron microscopy (TEM) imaging (Fig. 5a) and high-resolution TEM, (HRTEM) imaging (Fig. 5b) which is consistent with the XRD results. The FFT filtered image of the characteristic HRTEM micrograph of selected region (Fig. 5b) showed a very homogeneous nanostructure and no evidence for any phase separation was found in the amorphous SiCN ceramic matrix. At this stage, the SiCN nanostructure can be aptly called amorphous.

Thermolysis at high temperatures promotes structural reordering within the Si-C-N matrix. However, bright-field TEM imaging (Fig. 6a) and high-resolution TEM imaging (Fig. 6b) of the SiCN ceramics pyrolyzed at 1400 °C also exhibited no crystallinity. The incipient crystallization of  $\text{Si}_3\text{N}_4$ , as seen in the XRD, was not observed through TEM/HRTEM imaging, which may be due to the extremely low



**Figure 5** Electron microscopy of the SiCN ceramics; **a** TEM images and **b** HRTEM image of SiCN pyrolyzed at 1000 °C for 4 h. The inset is an FFT image of boxed region, which showed no evidence for any phase separation in the amorphous SiCN ceramic.

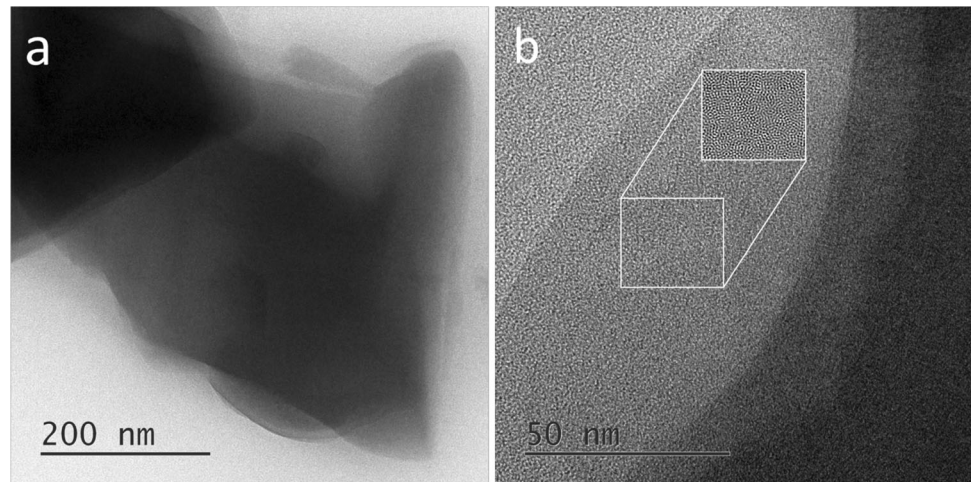
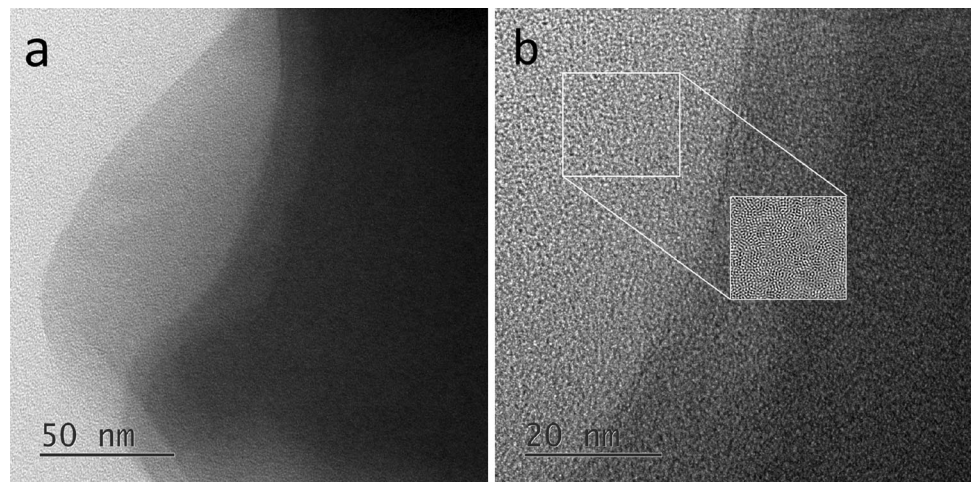


**Figure 6** Electron microscopy of the SiCN ceramics; **a** TEM images of 1400 °C pyrolyzed SiCN and corresponding SAED pattern in inset. **b** HRTEM image of SiCN pyrolyzed at 1400 °C. The inset is an FFT image of boxed region, which showed no evidence for any phase separation in SiCN ceramic as  $\text{Si}_3\text{N}_4$  or disordered graphite-like carbon.



volume fraction of such phases. Also, the inset FFT filtered image of characteristic HRTEM micrograph (Fig. 6b) of selected region showed a very homogeneous nanostructure and no evidence for any phase separation was observed in the SiCN microstructure in the form of  $\text{Si}_3\text{N}_4$  or disordered graphite-like carbon.

The selected area electron diffraction (SAED) pattern displayed in inset of Fig. 7a endorses its amorphous nature and is consistent with the X-ray diffractograms (Figs. 4 and 6). Further, we estimated the possible neighbor structural unit distances within the SiCN matrix through intensity profiles from the SAED pattern (Fig. 7b). To see the effect of Zr addition on the structural rearrangements within Si–C–N architectures, intensity profiles were also generated for the Zr modified PVS samples (Fig. 7d) of similar thermal history. These intensity profiles were plotted by the data obtained from calculation of average

radial intensity distribution of the SAED pattern from the center of the diffraction pattern (spatial frequency) followed by background subtraction with a second-order exponential decay function. Intensity profile of PVS-1400 sample (c.f. Figure 7b) shows most prominent spatial frequency peak, at  $2.44 \text{ nm}^{-1}$  (0.41 nm), which is assigned to the slightly disordered  $\text{SiN}_4$  tetrahedral units of mixed  $\text{SiC}_x\text{N}_y$ . The minor peak at  $3.23 \text{ nm}^{-1}$  (0.31 nm) is due to the presence of a small amount of the free carbon phase or mixed Si–C–N units that is commonly present in the high temperature pyrolyzed PDC ceramics. The maximum at  $5.42 \text{ nm}^{-1}$  (0.19 nm) corresponding to the tetrahedral  $\text{SiC}_4$  units and mixed Si–C–N units. In addition, the occurrence of peak at  $7.75 \text{ nm}^{-1}$  (0.13 nm) shows presence of tetrahedral  $\text{SiN}_4$  and  $\text{SiC}_4$  structural units of  $\text{SiC}_x\text{N}_y$ . Further spatial frequency peak cannot be assigned to any specific



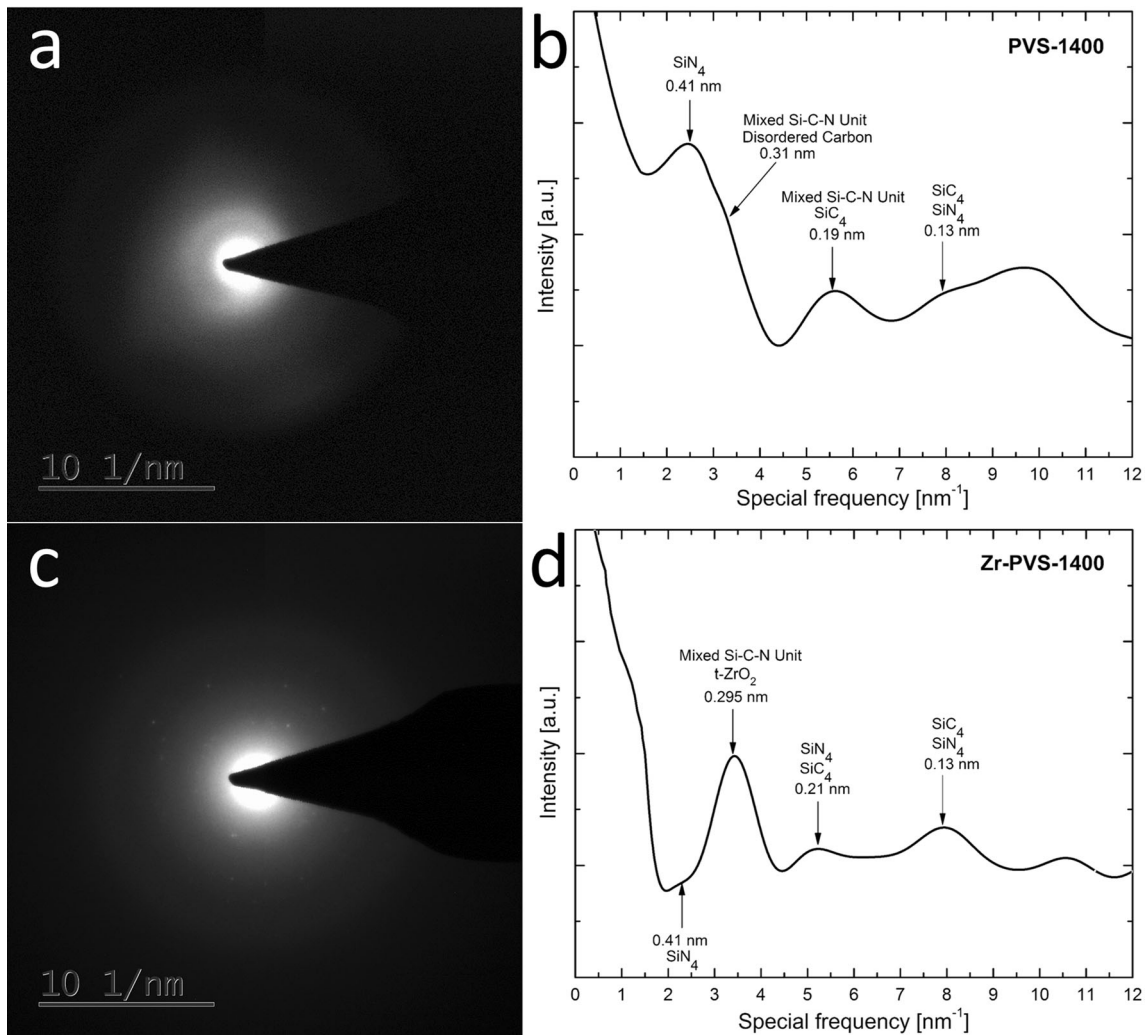


**Figure 7** **a** and **b** shows SAED patterns of the PVS-1400 and their corresponding estimated intensity profile. **c** and **d** shows SAED patterns of the Zr-PVS-1400 and their corresponding evaluated intensity profile.

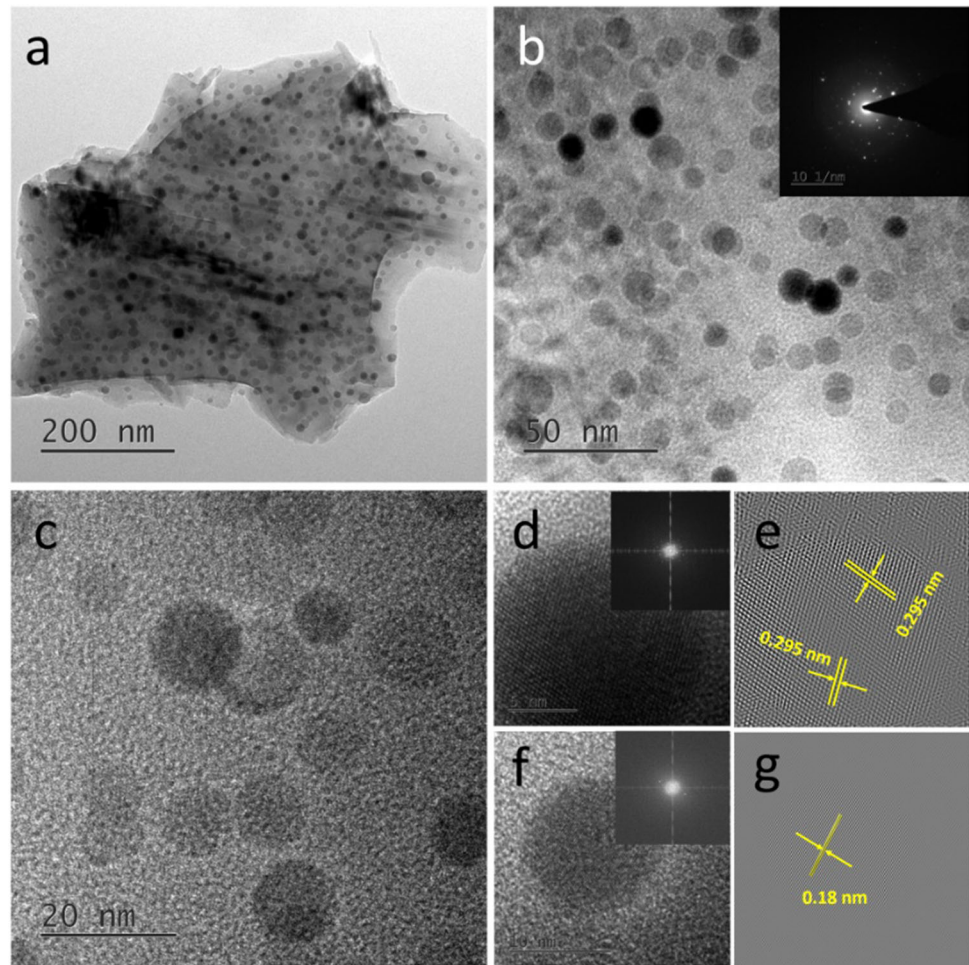
neighbors, since  $\text{SiC}_4$  and  $\text{SiN}_4$  units exhibit diffraction intensities largely in this range only.

Zr modified SiCN ceramics shows relatively sharp and more prominent special frequency peak at  $3.39 \text{ nm}^{-1}$  (0.295 nm), which can be assigned to (101) diffraction intensities of tetragonal  $\text{ZrO}_2$  and mixed Si-C-N units. Peaks at  $2.44 \text{ nm}^{-1}$ ,  $4.65 \text{ nm}^{-1}$  and  $7.75 \text{ nm}^{-1}$  confirm the disordered  $\text{SiN}_4$  units into  $\text{SiZr}_{0.2}\text{C}_x\text{N}_y$ . Also, the special frequency maxima at  $4.65 \text{ nm}^{-1}$  and  $7.75 \text{ nm}^{-1}$  shows presence of  $\text{SiC}_4$  units within Si-Zr-O-C-N architecture. However, a shift of the maximum spatial frequency peak from  $5.42 \text{ nm}^{-1}$  (0.19 nm) to  $4.65 \text{ nm}^{-1}$  (0.21 nm) indicates ordering of  $\text{SiC}_4$  units. It is noteworthy that there is no evidence of carbon in 1400 °C pyrolyzed Zr-PVS sample. It may be concluded that Zr doping into

SiCN ceramic modifies the structural rearrangement of  $\text{SiC}_x\text{N}_y$ , resulting in reduced amount of free carbon phase in the  $\text{SiZrCNO}$  system as compared to the pure SiCN system.

Additionally, the thermal stability and phase distribution of long annealed (1400 °C for 6 h)  $\text{SiZrCNO}$  ceramics were investigated through high-resolution TEM (Fig. 8). The bright-field TEM micrographs (cf. Figure 8a and b) clearly exhibit that the continuous and uniform dispersion of nanocrystallites throughout the SiCN ceramic matrix is still maintained. Clearer patterns can now be seen on the SAED profile shown in the inset of Fig. 8b. Figure 8c shows the high-resolution micrographs of the samples annealed at 1400 °C for 6 h. In the HRTEM image of this sample (Fig. 8d and f), crystallization of t- $\text{ZrO}_2$

**Figure 8** Electron microscopy of SiZrCNO ceramics annealed at 1400 °C, 6 Hours; **a** bright-field TEM micrograph showing nanocrystals dispersed into SiCN matrix, **b** magnified TEM micrograph, inset image is of corresponding SAED pattern. **c** HRTEM micrograph showing nanostructured t-ZrO<sub>2</sub> dispersed into SiCN matrix, **d** 5 nm magnified HRTEM image, inset image shows corresponding FFT planes, **e** Inverse FFT image confirming the crystal lattice of the nanostructured t-ZrO<sub>2</sub>. **f** 10 nm magnified HRTEM image, inset image shows corresponding FFT planes, and **g** Inverse FFT image confirming the crystal lattice of the nanostructured t-ZrO<sub>2</sub>.



crystals is clearly observed. Inverse FFT images (Fig. 8e and g) corresponding to patterns inserted in Fig. 8d and f confirming (101) and (112) planes, respectively. At 6 h of annealing, the t-ZrO<sub>2</sub> crystallites appear to have grown fast to sizes in the range of 10–12 nm. However, no crystalline phases other than t-ZrO<sub>2</sub> was identified in the HRTEM micrographs, and no phase transformation of t-ZrO<sub>2</sub> was observed in the SiZrCNO ceramic. At this stage, the SiZrCNO system can be appropriately called a nanocomposite of SiCN-ZrO<sub>2</sub>.

It is remarkable to note that the stability of tetragonal form of ZrO<sub>2</sub> and ternary SiCN has been observed at high temperatures, such as 1400 °C. In the ZrO<sub>2</sub> nanoparticle filled SiOC system, major phase of zirconia was reported to be monoclinic even at lower pyrolysis temperature (~ 1100 °C) [26]. Dire et al. [40] investigated phase evolution and crystallization behavior of polydimethylsiloxane-zirconia nanocomposite and reported finely dispersed

t-ZrO<sub>2</sub> particles dispersed in an amorphous SiCO matrix, while at 1400 °C, a mixture of monoclinic and tetragonal phase of ZrO<sub>2</sub> was observed. In the Hf-doped SiCNO system, pyrolysis above 1000 °C led to the formation of t-HfO<sub>2</sub> phase [51]. However, at 1400 °C for just 5 h annealing, a fraction of tetragonal HfO<sub>2</sub> converted to monoclinic phase generating microstrain in the system. Nevertheless, in this work, we have successively stabilized the metastable tetragonal polymorph of zirconia even up to temperatures as high as 1400 °C, which ensures thermal stability of the SiZrCNO system.

The phase transformation of t-ZrO<sub>2</sub> depends on the particle morphology, size, shape, and location (intra/intergranular). Ushakov et al. [52] investigated amorphous to crystalline transformation temperature of zirconia in related system like SiO<sub>2</sub> and concluded that transformation temperature into other polymorphs increases by more than 300 °C with the increase in surface/interface area of the t-ZrO<sub>2</sub> phase.

The fact that the t-ZrO<sub>2</sub> crystallites in our experiments were of extremely fine dimension, the heterophase interface area is much higher, which according to Ushakov et al. might increase the transformation temperature considerably. Additionally, the diffusion rate of oxygen is significantly hindered in the SiCN matrix system, as compared to SiO<sub>2</sub>, due to the presence of carbon and nitrogen. As a result, the coarsening rate of ZrO<sub>2</sub> is retarded, which leads to sustenance of the fine crystallite size and stability of the t-ZrO<sub>2</sub> phase [31, 53–55]. The much lowered surface energy of the t-ZrO<sub>2</sub>/SiCN interface may also be a reason for a lower free energy of the system. In the absence of a stabilizer, for the t-ZrO<sub>2</sub> phase to be stable, the crystallite size of the phase should remain below about 30 nm [56]. The t-ZrO<sub>2</sub> nanocrystals size in the current work (across all histories of pyrolysis) remained much lower (< 12 nm) than the critical size for tetragonal to monoclinic transformation. High-resolution TEM images exhibited that the nucleation and growth of t-ZrO<sub>2</sub> in SiCN glassy matrix produces spherical or ellipsoidal crystals without any sharp edges (c.f. Figure 8 b, c, d, and f). Precipitates with sharp and leading edges ordinarily act as potential stress concentrators, lack of which can be a reason for the absence of polymorphic transformations in the current investigation. Furthermore, t-ZrO<sub>2</sub> can be stabilized by large strain energy which would be relieved by the volume increase associated with the t-m transformation. The mismatch in the coefficient of thermal expansion imposes a compressive stress on the t-ZrO<sub>2</sub>. Moreover, the SiCN glass matrix suppresses t-m ZrO<sub>2</sub> polymorph conversion by constraining the volume expansion of the embedded ZrO<sub>2</sub> particles ( $\alpha_{\text{SiCN}} = 3.08 - 3.96 \times 10^{-6} \text{ K}^{-1}$ ,  $\alpha_{\text{t-ZrO}_2} = 11.6 \times 10^{-6} / \text{K}^{-1}$  and  $16.08 \times 10^{-6} \text{ K}^{-1}$  in a and c axis, respectively) [57, 58]. Thus, several factors are responsible for the stabilization of extremely fine crystallites of t-ZrO<sub>2</sub> in the SiCN amorphous matrix.

High temperature induced oxidation or materials recession resistance is an important characteristic of bond coat materials for environmental barrier coatings. While the SiCN-ZrO<sub>2</sub> system is being investigated as an intermediate layer mainly for its uniformity in microstructure containing two different phases of widely different CTE, some extent of oxygen ingress can be expected beneath the topcoat. Therefore, to test the oxidation resistance, we have performed thermogravimetry-based evaluation. Finely ground ceramic powders of SiCN and SiCN-

ZrO<sub>2</sub> were heated with a constant heating rate in flowing oxygen atmosphere while performing gravimetry. This method can be a more aggressive way of testing the oxidation resistance of the ceramics in a short span of time. As compared to a ceramic coating, the current experiments expose the fine ceramic powders to a more intense oxygen attack (from all sides of the particulate). Figure 9 shows the effect of Zr doping into SiCN ceramic on the oxidation behavior. This has been compared with the oxidation test conducted on pure SiCN ceramic for benchmarking. The TG measurements up to 1500 °C in oxidizing atmosphere show a total mass loss of 9.54% and 6.54% for undoped SiCN and Zr-doped SiCN ceramics, respectively. Up to 1150 °C, the SiCN-1400 and SiZrCNO-1400 systems show 2.1% and 0.8% mass loss, respectively. These, initial losses in both the systems are mainly due to the presence of residual carbon in the ceramic matrices, with the conversion of C to CO and/or CO<sub>2</sub>. The presence of the residual carbon in the ceramic matrix in pyrolyzed SiCN-1400 and SiZrCNO-1400 samples could be established from the Raman spectrum. Figure 10 shows typical Raman spectrum of pure and Zr-modified SiCN synthesized at 1400 °C before and after oxidation at 1400 °C for 2 h. The typical D & G absorption bands observed at 1350 and 1610 cm<sup>-1</sup> indicate the presence of free carbon. Under ambient condition, this free carbon would oxidize easily. Generally, a free carbon form (such as graphite, graphene, or graphene oxide) can oxidize in the

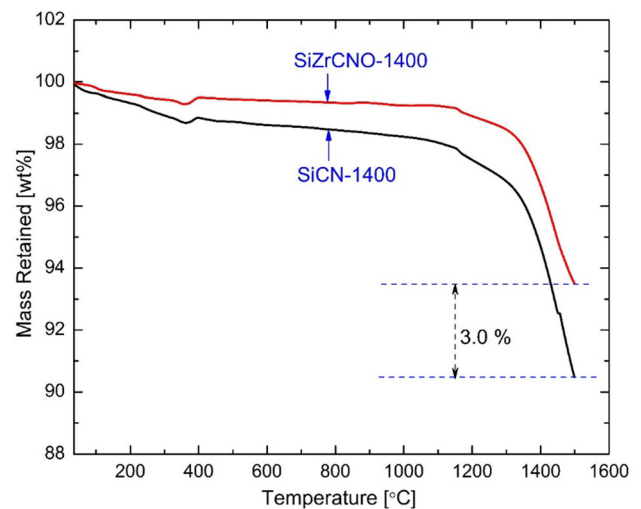


**Figure 9** Thermogravimetric oxidation curve of pure and Zr modified SiCN ceramics pyrolyzed at 1400 °C.



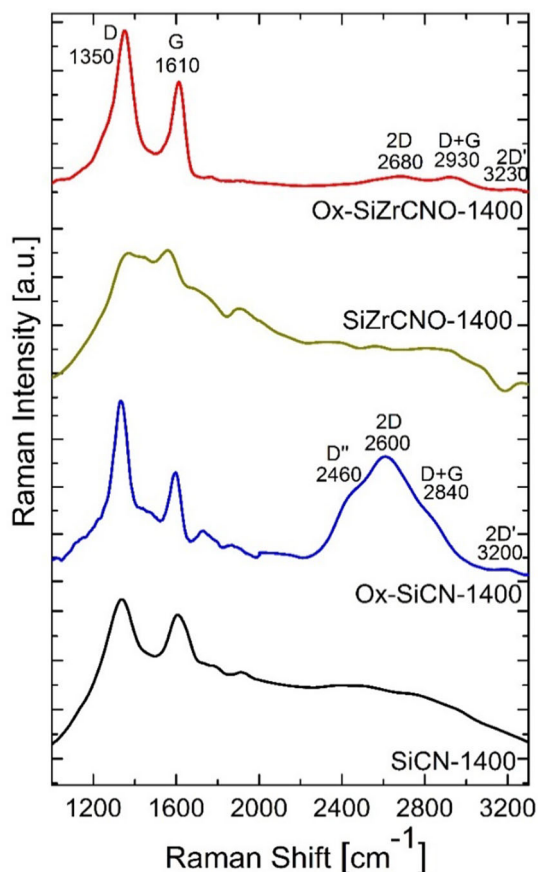


**Figure 10** Raman spectra of pyrolyzed SiCN-1400 and SiZrCNO-1400 samples before and after oxidation showing D, G, D<sup>''</sup>, 2D, D+G and 2D' peaks.

temperature range of 400 °C to 800 °C. However, the free carbon phase in the SiCN is embedded in the amorphous ceramic nanostructure itself, where it is protected by the ceramic, and the oxidation temperature shifts above 1150 °C. Yet, the undoped SiCN sample suffers continuous mass loss of 7.4% from 1150 to 1500 °C. The high partial pressure of O<sub>2</sub> in the system may induce phase separation of the SiCN amorphous ceramic to crystallize SiO<sub>2</sub>, free C, and N<sub>2</sub> gas. The evolved N<sub>2</sub> gas leaves the system causing weight loss. The evolved free carbon could be characterized by the prominent Raman peak appearances of D, G, D<sup>''</sup>, 2D, D+G and 2D' bands of oxidized SiCN-1400 and SiZrCNO-1400 samples (Fig. 10). The free C phase oxidizes to CO<sub>2</sub>, and creates pore channels within the structure, which further exposes the carbon and nitrogen sites, and accelerates oxygen diffusion into the SiCN matrix. Additionally, the free C phase may also react with trace amounts of Si<sub>3</sub>N<sub>4</sub> in the system to produce SiC and N<sub>2</sub> (the latter of which

leaves the system causing mass loss). In dry air condition, the SiC phase present may react with O<sub>2</sub> to form SiO<sub>2</sub> which typically acts as a coating thus preventing further oxidation. Moreover, materials recession can also occur due to the direct contact of free C with SiO<sub>2</sub>, resulting in dissociation of SiO<sub>2</sub> into gaseous SiO and CO.

Incorporation of Zr in the SiCN matrix, the mass loss after oxidation of the SiZrCNO reduces by 3.0%. The reduced mass loss may be attributed to the lower amount of free carbon present in the SiZrCNO ceramics than undoped SiCN system (Figs. 1, 7 and 10). Zr-doping in oxycarbide ceramic system has been found to retard crystallization as well as phase separation of the carbon phase and SiO<sub>2</sub> from the pyrolyzed PDCs system [27]. It can also be referred from the XRD patterns (Fig. 4) that the corresponding peak intensity of the  $\alpha$ -Si<sub>3</sub>N<sub>4</sub> phase is relatively higher for the 1400 °C pyrolyzed SiZrCNO as compared to SiCN indicating that the phase separation of Si<sub>3</sub>N<sub>4</sub> from the SiCN system is favored upon Zr doping. Si<sub>3</sub>N<sub>4</sub> shows slightly better oxidation resistance than SiC and SiCN system, and hence, it also retards the oxidation of SiZrCNO system [59]. Further, the evolved ZrO<sub>2</sub> phase throughout the SiCN matrix acts as barrier and retards the diffusivity of oxygen into the SiZrCNO ceramics. The mass loss of SiZrCNO is less than the SiC, SiOC, SiTiOC, as well as SiCN, systems in oxygen atmosphere, making it robust against oxidation [25]. Also, comparison of results of similar systems, in particular for SiCNO and SiHfCNO reported by Sujith et al. [60], with current results shows a clearly reduced materials recession for pure SiCN and SiZrCNO (Table 1).

**Table 1** Mass loss (%) upon annealing at various temperatures between 1200 and 1500 °C in air

PDC	1200 °C	1400 °C	1500 °C	References
SiCNO	+ 16	– 6	–	[60]
SiHfCNO	– 5	– 11	– 15	[60]
SiCN	– 2.5	– 5.3	– 9.5	Present Work
SiZrCNO	– 1.1	– 3.4	– 6.5	Present Work

+ and – point to mass gain, and mass loss respectively



## Summary

SiCN and SiZrCNO ceramics were prepared from polyvinylsilazane-based preceramic polymers, without and with Zr-doping, respectively. Presence of the Zr-O-Si and Zr-O bands exhibited through FTIR confirmed doping of Zr at molecular level and the incorporation of Zr in the main polymer chain of polyvinylsilazane precursor. An important outcome of the work is that the Zr doping accelerates polymer to ceramic transformation and shifts the ceramization temperature to 700 °C from 800 °C. The pure SiCN ceramic was stable and pseudo-amorphous up to the pyrolysis temperature of 1400 °C. The Zr-doped SiCN ceramic appeared as monophasic non-crystalline ceramic at 1000 °C and exhibited phase separation of Zr into nanocrystals of t-ZrO<sub>2</sub> at 1200 °C onwards. For the SiCN and SiZrCNO sample pyrolyzed at 1400 °C, the presence of faint peaks of residual graphitic carbon and nanocrystalline  $\alpha$ -Si<sub>3</sub>N<sub>4</sub> was observed in XRD analysis. The distribution of t-ZrO<sub>2</sub> crystallites in the 5–12 nm range appeared exceptionally uniform throughout the SiZrCNO matrix. From XRD, TEM, and intensity profiles, it could be further understood that the retention of SiCN matrix as well as tetragonal phase of nanocrystalline ZrO<sub>2</sub>, even after prolonged heat treatment at 1400 °C, provides a significant advantage for the ceramic in high temperature structural applications. Extremely fine size (less than the critical size), spherical or ellipsoidal crystal shapes without any sharp edges, low t-ZrO<sub>2</sub>/SiCN interface energy and SiCN glassy matrix system were the reasons for the exceptional stability of metastable t-ZrO<sub>2</sub> in the SiZrCNO ceramics. Constant heating rate oxidation tests revealed improved oxidation behavior of SiCN-ZrO<sub>2</sub> ceramic system with 3% reduced mass loss as compared to the pure SiCN ceramic. These findings will allow the fabrication of a bond coat material with better toughness, oxidation resistance, hot strength, and tailorable thermal expansion coefficient, to match between SiC-based ceramic matrix composite substrates and oxide/silicate-based topcoats.

## References

- [1] Padture NP (2016) Advanced structural ceramics in aerospace propulsion. *Nat Mater* 15(8):804–809. <https://doi.org/10.1038/nmat4687>
- [2] Marshall DB, Cox BN (2008) Integral textile ceramic structures. *Annu Rev Mater Res* 38(1):425–443. <https://doi.org/10.1146/annurev.matsci.38.060407.130214>
- [3] Flores O, Bordia RK, Nestler D, Krenkel W, Motz G (2014) Ceramic fibers based on SiC and SiCN systems: current research, development, and commercial status. *Adv Eng Mater* 16(6):621–636. <https://doi.org/10.1002/adem.201400069>
- [4] Ren Z, Singh G (2019) Nonoxide polymer-derived CMCs for “super” turbines. *Am Ceram Soc Bull*, 98 (3):34–39. <https://par.nsf.gov/biblio/10108196>
- [5] Sudhir B, Raj R (2006) Effect of steam velocity on the hydrothermal oxidation/volatilization of silicon nitride. *J Am Ceram Soc* 89(4):1380–1387. <https://doi.org/10.1111/j.1551-2916.2005.00907.x>
- [6] Meschter PJ, Opila EJ, Jacobson NS (2013) Water vapor-mediated volatilization of high-temperature materials. *Annu Rev Mater Res* 43(1):559–588. <https://doi.org/10.1146/annurev-matsci-071312-121636>
- [7] Turcer LR, Padture NP (2018) Towards multifunctional thermal environmental barrier coatings (TEBCs) based on rare-earth pyrosilicate solid-solution ceramics. *Scr Mater* 154:111–117. <https://doi.org/10.1016/j.scriptamat.2018.05.032>
- [8] Fritsch M, Klemm H, Herrmann M, Schenk B (2006) Corrosion of selected ceramic materials in hot gas environment. *J Eur Ceram Soc* 26(16):3557–3565. <https://doi.org/10.1016/j.jeurceramsoc.2006.01.015>
- [9] Riedel R, Kienzle A, Dressler W, Ruwisch L, Bill J, Aldinger F (1996) A silicoboron carbonitride ceramic stable to 2000°C. *Nature* 382:796. <https://doi.org/10.1038/382796a0>
- [10] Bharadwaj L, Fan Y, Zhang L, Jiang D, An L (2004) Oxidation behavior of a fully dense polymer-derived amorphous silicon carbonitride ceramic. *J Am Ceram Soc* 87(3):483–486. <https://doi.org/10.1111/j.1551-2916.2004.00483.x>
- [11] Riedel R, Mera G, Hauser R, Klonczynski A (2006) Silicon-based polymer-derived ceramics: synthesis properties and applications—a review. *J Ceram Soc JAPAN* 114(1330):425–444. <https://doi.org/10.2109/jcersj.114.425>

- [12] Emanuel I, Gabriela M, Ralf R (2013) Polymer-derived ceramics (PDCs): materials design towards applications at ultrahigh-temperatures and in extreme environments. In: Low IM, Sakka Y, Hu CF (eds) MAX phases and ultra-high temperature ceramics for extreme environments. IGI Global, Hershey
- [13] Saha A, Shah SR, Raj R (2004) Oxidation behavior of SiCN–ZrO<sub>2</sub> fiber prepared from alkoxide-modified silazane. *J Am Ceram Soc* 87(8):1556–1558. <https://doi.org/10.1111/j.1551-2916.2004.01556.x>
- [14] Shah SR, Raj R (2001) Nanoscale densification creep in polymer-derived silicon carbonitrides at 1350°C. *J Am Ceram Soc* 84(10):2208–2212. <https://doi.org/10.1111/j.1151-2916.2001.tb00989.x>
- [15] Paolo C, Gabriela M, Ralf R, Domenico SG (2010) Polymer-derived ceramics: 40 years of research and innovation in advanced ceramics. *J Am Ceram Soc* 93(7):1805–1837. <https://doi.org/10.1111/j.1551-2916.2010.03876.x>
- [16] Saha A, Raj R, Williamson DL, Kleebe HJ (2005) Characterization of nanodomains in polymer-derived SiCN ceramics employing multiple techniques. *J Am Ceram Soc* 88(1):232–234. <https://doi.org/10.1111/j.1551-2916.2004.00034.x>
- [17] Kleebe HJ, Störmer H, Trassl S, Ziegler G (2001) Thermal stability of SiCN ceramics studied by spectroscopy and electron microscopy. *Appl Organomet Chem* 15(10):858–866. <https://doi.org/10.1002/aoc.243>
- [18] Kleebe HJ (1998) Microstructure and stability of polymer-derived ceramics; the Si–C–N system. *Phys Status Solidi (a)* 166(1):297–313. [https://doi.org/10.1002/\(SICI\)1521-396X\(199803\)166:1%3c297::AID-PSSA297%3e3.0.CO;2-3](https://doi.org/10.1002/(SICI)1521-396X(199803)166:1%3c297::AID-PSSA297%3e3.0.CO;2-3)
- [19] Riedel R, Passing G, Schonfelder H, Brook RJ (1992) Synthesis of dense silicon-based ceramics at low temperatures. *Nature* 355(6362):714–717. <https://doi.org/10.1038/55714a0>
- [20] Riedel R, Kleebe H-J, Schonfelder H, Aldinger F (1995) A covalent micro/nano-composite resistant to high-temperature oxidation. *Nature* 374(6522):526–528. <https://doi.org/10.1038/374526a0>
- [21] Mera G, Riedel R, Poli F, Müller K (2009) Carbon-rich SiCN ceramics derived from phenyl-containing poly(silyl-carbodiimides). *J Eur Ceram Soc* 29(13):2873–2883. <https://doi.org/10.1016/j.jeurceramsoc.2009.03.026>
- [22] Martin H-P, Müller E, Irmer G, Babonneau F (1997) Crystallisation behaviour and polytype transformation of polymer-derived silicon carbide. *J Eur Ceram Soc* 17(5):659–666. [https://doi.org/10.1016/S0955-2219\(96\)00117-3](https://doi.org/10.1016/S0955-2219(96)00117-3)
- [23] Iwamoto Y, Völger W, Kroke E, Riedel R, Saitou T, Matsunaga K (2001) Crystallization behavior of amorphous silicon carbonitride ceramics derived from organometallic precursors. *J Am Ceram Soc* 84(10):2170–2178. <https://doi.org/10.1111/j.1151-2916.2001.tb00983.x>
- [24] Saha A, Raj R (2007) Crystallization maps for SiCO amorphous ceramics. *J Am Ceram Soc* 90(2):578–583. <https://doi.org/10.1111/j.1551-2916.2006.01423.x>
- [25] Anand R, Sahoo SP, Nayak BB, Behera SK (2019) Phase evolution, nanostructure, and oxidation resistance of polymer derived SiTiOC ceramic hybrid. *Ceram Int* 45(5):6570–6576. <https://doi.org/10.1016/j.ceramint.2018.12.024>
- [26] Ionescu E, Linck C, Fasel C, Müller M, Kleebe HJ, Riedel R (2010) Polymer-derived SiOC/ZrO<sub>2</sub> ceramic nanocomposites with excellent high-temperature stability. *J Am Ceram Soc* 93(1):241–250. <https://doi.org/10.1111/j.1551-2916.2009.03395.x>
- [27] Anand R, Sahoo SP, Nayak BB, Behera SK (2020) Phase evolution in Zr-doped preceramic polymer derived SiZrOC hybrids. *Ceram Int* 46(7):9962–9967. <https://doi.org/10.1016/j.ceramint.2019.12.196>
- [28] Linck C, Ionescu E, Papendorf B, Galuskova D, Galusek D, Šajgalik P, Riedel R (2012) Corrosion behavior of silicon oxycarbide-based ceramic nanocomposites under hydrothermal conditions. *Int J Mater Res* 103(1):31–39. <https://doi.org/10.3139/146.110625>
- [29] Terauds K, Raj R (2013) Limits to the stability of the amorphous nature of polymer-derived HfSiCNO compounds. *J Am Ceram Soc* 96(7):2117–2123. <https://doi.org/10.1111/jace.12382>
- [30] Terauds K, Marshall DB, Raj R (2013) Oxidation of polymer-derived HfSiCNO up to 1600°C. *J Am Ceram Soc* 96(4):1278–1284. <https://doi.org/10.1111/jace.12239>
- [31] Anand R, Nayak BB, Behera SK (2019) Coarsening kinetics of nanostructured ZrO<sub>2</sub> in Zr-doped SiCN ceramic hybrids. *J Alloys Compd* 811:151939. <https://doi.org/10.1016/j.jallcom.2019.151939>
- [32] Saha A, Shah SR, Raj R (2003) Amorphous silicon carbonitride fibers drawn from alkoxide modified ceraset<sup>TM</sup>. *J Am Ceram Soc* 86(8):1443–1445. <https://doi.org/10.1111/j.1151-2916.2003.tb03493.x>
- [33] Sun J, Li T, Reitz A, Fu Q, Riedel R, Yu Z (2020) High-temperature stability and oxidation behavior of SiOC/HfO<sub>2</sub> ceramic nanocomposite in air. *Corros Sci* 175:108866. <https://doi.org/10.1016/j.corsci.2020.108866>
- [34] King A, Singh R, Nayak BB (2020) Synthesis and photoluminescence behaviour of ultra-fine particles of Eu-doped zirconia nanopowders. *J Solid State Chem* 282:121106. <https://doi.org/10.1016/j.jssc.2019.121106>
- [35] Hannink RHJ, Kelly PM, Muddle BC (2000) Transformation toughening in zirconia-containing ceramics. *J Am Ceram*

- Soc 83(3):461–487. <https://doi.org/10.1111/j.1151-2916.2000.tb01221.x>
- [36] Wang X, Schmidt F, Hanaor D, Kamm PH, Li S, Gurlo A (2019) Additive manufacturing of ceramics from preceramic polymers: A versatile stereolithographic approach assisted by thiol-ene click chemistry. *Addit Manuf* 27:80–90. <https://doi.org/10.1016/j.addma.2019.02.012>
- [37] Sorarù GD, Pederiva L, Latournerie J, Raj R (2002) Pyrolysis kinetics for the conversion of a polymer into an amorphous silicon oxycarbide ceramic. *J Am Ceram Soc* 85(9):2181–2187. <https://doi.org/10.1111/j.1151-2916.2002.tb00432.x>
- [38] Wrobel AM, Uznanski P, Walkiewicz-Pietrzykowska A, Jankowski K (2017) Amorphous silicon carbonitride thin-film coatings produced by remote nitrogen microwave plasma chemical vapour deposition using organosilicon precursor. *Appl Organomet Chem* 31(12):e3871. <https://doi.org/10.1002/aoc.3871>
- [39] Shah SR, Raj R (2002) Mechanical properties of a fully dense polymer derived ceramic made by a novel pressure casting process. *Acta Mater* 50(16):4093–4103. [https://doi.org/10.1016/S1359-6454\(02\)00206-9](https://doi.org/10.1016/S1359-6454(02)00206-9)
- [40] Dirè S, Ceccato R, Gialanella S, Babonneau F (1999) Thermal evolution and crystallisation of polydimethylsiloxane–zirconia nanocomposites prepared by the sol–gel method. *J Eur Ceram Soc* 19(16):2849–2858. [https://doi.org/10.1016/S0955-2219\(99\)00063-1](https://doi.org/10.1016/S0955-2219(99)00063-1)
- [41] Liu C, Pan R, Hong C, Zhang X, Han W, Han J, Du S (2016) Effects of Zr on the precursor architecture and high-temperature nanostructure evolution of SiOC polymer-derived ceramics. *J Eur Ceram Soc* 36(3):395–402. <https://doi.org/10.1016/j.jeurceramsoc.2015.09.009>
- [42] Kaufman JH, Metin S, Saperstein DD (1989) Symmetry breaking in nitrogen-doped amorphous carbon: Infrared observation of the Raman-active G and D bands. *Phys Rev B* 39(18):13053–13060
- [43] Bouchet-Fabre B, Marino E, Lazar G, Zellama K, Clin M, Ballutaud D, Abel F, Godet C (2005) Spectroscopic study using FTIR, Raman, XPS and NEXAFS of carbon nitride thin films deposited by RF magnetron sputtering. *Thin Solid Films* 482(1):167–171. <https://doi.org/10.1016/j.tsf.2004.11.166>
- [44] Xiao X-c, Li Y-w, Song L-x, Peng X-f, Hu X-f (2000) Structural analysis and microstructural observation of SiC<sub>x</sub>N<sub>y</sub> films prepared by reactive sputtering of SiC in N<sub>2</sub> and Ar. *Appl Surf Sci* 156(1):155–160. [https://doi.org/10.1016/S0169-4332\(99\)00493-6](https://doi.org/10.1016/S0169-4332(99)00493-6)
- [45] Bulou S, Le Brizoual L, Miska P, de Poucques L, Hugon R, Belmahi M, Bougdira J (2011) The influence of CH<sub>4</sub> addition on composition, structure and optical characteristics of SiCN thin films deposited in a CH<sub>4</sub>/N<sub>2</sub>/Ar/hexamethyldisilazane microwave plasma. *Thin Solid Films* 520(1):245–250. <https://doi.org/10.1016/j.tsf.2011.07.054>
- [46] Zhao JP, Chen ZY, Yano T, Ooie T, Yoneda M, Sakakibara J (2001) Structural and bonding properties of carbon nitride films synthesized by low energy nitrogen-ion-beam-assisted pulsed laser deposition with different laser fluences. *J Appl Phys* 89(3):1634–1640. <https://doi.org/10.1063/1.1334643>
- [47] Besling WFA, Goossens A, Meester B, Schoonman J (1998) Laser-induced chemical vapor deposition of nanostructured silicon carbonitride thin films. *J Appl Phys* 83(1):544–553. <https://doi.org/10.1063/1.366669>
- [48] Jędrzejowski P, Cizek J, Amassian A, Klemberg-Sapieha JE, Vlcek J, Martinu L (2004) Mechanical and optical properties of hard SiCN coatings prepared by PECVD. *Thin Solid Films*. [https://doi.org/10.1016/S0040-6090\(03\)01057-5](https://doi.org/10.1016/S0040-6090(03)01057-5)
- [49] Silva JA, Quoizola S, Hernandez E, Thomas L, Massines F (2014) Silicon carbon nitride films as passivation and antireflective coatings for silicon solar cells. *Surf Coat Technol*. <https://doi.org/10.1016/j.surfcoat.2014.01.037>
- [50] Ay F, Aydinli A (2004) Comparative investigation of hydrogen bonding in silicon based PECVD grown dielectrics for optical waveguides. *Opt Mater* 26(1):33–46. <https://doi.org/10.1016/j.optmat.2003.12.004>
- [51] Sujith R, Kousaalya AB, Kumar R (2011) Coarsening induced phase transformation of hafnia in polymer-derived Si–Hf–C–N–O ceramics. *J Am Ceram Soc* 94(9):2788–2791. <https://doi.org/10.1111/j.1551-2916.2011.04719.x>
- [52] Ushakov SV, Navrotsky A, Yang Y, Stemmer S, Kukli K, Ritala M, Leskelä MA, Fejes P, Demkov A, Wang C, Nguyen B-Y, Triyoso D, Tobin P (2004) Crystallization in hafnia- and zirconia-based systems. *Phys Status Solidi (b)*. <https://doi.org/10.1002/pssb.200404935>
- [53] Yamaoka M, Murakami H, Miyazaki S (2003) Diffusion and incorporation of Zr into thermally grown SiO<sub>2</sub> on Si(1 0 0). *Appl Surf Sci* 216(1):223–227. [https://doi.org/10.1016/S0169-4332\(03\)00428-8](https://doi.org/10.1016/S0169-4332(03)00428-8)
- [54] Kleebe H-J, Nonnenmacher K, Ionescu E, Riedel R (2012) Decomposition-coarsening model of SiOC/HfO<sub>2</sub> ceramic nanocomposites upon isothermal anneal at 1300°C. *J Am Ceram Soc* 95(7):2290–2297. <https://doi.org/10.1111/j.1551-2916.2012.05227.x>
- [55] Ikarashi N, Watanabe K, Masuzaki K, Nakagawa T, Miyamura M (2006) The influence of incorporated nitrogen on the thermal stability of amorphous HfO<sub>2</sub> and Hf silicate. *J Appl Phys* 100(6):063507. <https://doi.org/10.1063/1.2353262>
- [56] Garvie RC (1965) The occurrence of metastable tetragonal zirconia as a crystallite size effect. *J Phys Chem* 69(4):1238–1243. <https://doi.org/10.1021/j100888a024>

- [57] Nishimura T, Haug R, Bill J, Thurn G, Aldinger F (1998) Mechanical and thermal properties of Si–C–N material from polyvinylsilazane. *J Mater Sci* 33(21):5237–5241. <https://doi.org/10.1023/a:1004440122266>
- [58] Patil RN, Subbarao EC (1969) Axial thermal expansion of ZrO<sub>2</sub> and HfO<sub>2</sub> in the range room temperature to 1400°C. *J Appl Crystallogr* 2(6):281–288. <https://doi.org/10.1107/s0021889869007217>
- [59] Mocaer D, Chollon G, Paillet R, Filipuzzi L, Naslain R (1993) Si-C-N ceramics with a high microstructural stability elaborated from the pyrolysis of new polycarbosilazane precursors. *J Mater Sci* 28(11):3059–3068. <https://doi.org/10.1007/bf00354712>
- [60] Sujith R, Kousaalya AB, Kumar R (2012) Synthesis and phase stability of precursor derived HfO<sub>2</sub>/Si–C–N–O nanocomposites. *Ceram Int* 38(2):1227–1233. <https://doi.org/10.1016/j.ceramint.2011.08.053>

**Publisher's Note** Springer Nature remains neutral with regard to jurisdictional claims in published maps and institutional affiliations.